NANO LETTERS

Letter

pubs.acs.org/NanoLett

Subgroup Decomposition of Plasmonic Resonances in Hybrid Oligomers: Modeling the Resonance Lineshape

Mohsen Rahmani,[†,‡,¶] Dang Yuan Lei,[§,¶] Vincenzo Giannini,[§] Boris Lukiyanchuk,[†] Mojtaba Ranjbar,[†,‡] Thomas Yun Fook Liew,[†,‡] Minghui Hong,[†,‡,*] and Stefan A. Maier[§,*]

[†]Data Storage Institute, (A*STAR) Agency for Science, Technology and Research, 5 Engineering Drive 1, Singapore 117608

[‡]Department of Electrical and Computer Engineering, National University of Singapore, 4 Engineering Drive 3, Singapore 117576

[§]Department of Physics, Imperial College London, London SW7 2AZ, United Kingdom

ABSTRACT: Plasmonic resonances with a Fano lineshape observed in metallic nanoclusters often arise from the destructive interference between a dark, subradiant mode and a bright, super-radiant one. A flexible control over the Fano profile characterized by its linewidth and spectral contrast is crucial for many potential applications such as slowing light and biosensing. In this work, we show how one can easily but significantly tailor the overall spectral profile in plasmonic nanocluster systems, for example, quadrumers and pentamers, by selectively altering the particle shape without a need to change the particle size, interparticle distance, or the number of elements of the oligomers. This is achieved through decomposing the whole spectrum into two separate contributions from subgroups, which are efficiently excited at their spectral peak positions. We further show that different strengths of interference between the two subgroups must be considered for a full understanding of the resulting spectral lineshape. In some cases, each subgroup is separately active in distinct frequency windows with only small overlap, leading to a simple convolution of the subspectra. Variation in particle shape of either subgroup results in the tuning of the overall spectral lineshape, which opens a novel pathway for shaping the plasmonic response in small nanoclusters.

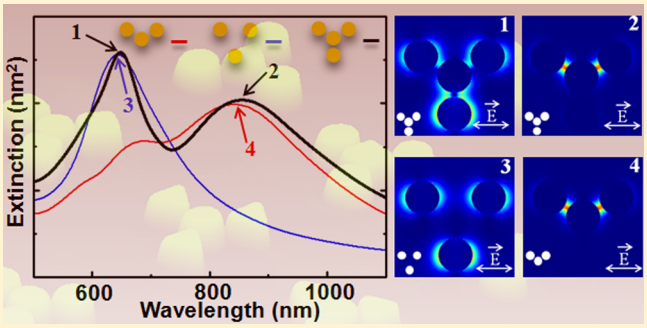

KEYWORDS: *Subwavelength nanostructures, surface plasmons, Fano resonances, plasmonic oligomers, subgroup decomposition*

Since Ugo Fano theoretically described the distinctly asymmetric absorption profile[1] experimentally observed in noble gases,[2] Fano interferences have been applied successfully to explain a large number of phenomena in various systems. These phenomena include the autoionization of atoms,[2] resonant interference in Raman spectra of single crystals,[3] energy-dependent line profiles of absorption in molecular systems,[4] asymmetric distributions of the density of states in Anderson impurity systems,[5] quantum transport in quantum dots and quantum wires[6,7] and strong coupling between Mie and Bragg scattering in photonic crystals.[8] A common feature shared by these observations is the overlap of a discrete state with a continuum state where destructive and constructive interferences take place at close energy positions, which results in the asymmetric profile. A comprehensive description of Fano theory and its applications can be found in recent reviews by Miroshnichenko and Luk'yanchuk.[9,10]

Metallic nanostructures can sustain surface plasmons which are coherent oscillations of the conduction electrons at the interface between metal and dielectric materials.[11] Recently, plasmon resonances with a Fano lineshape have also been observed in various metallic nanostructures exhibiting strongly plasmonic hybridized modes,[12−31] and this is driving strong efforts in theoretical plasmonics in order to carefully describe such phenomena.[30] For example, strong coupling between localized surface plasmons and optical waveguide modes results in a distinctly asymmetric lineshape of transmission through metallic nanowire arrays on dielectric waveguide substrates.[12] The interference between a resonant surface plasmon excitation and a nonresonant direct scattering reasonably accounts for the red shift and asymmetric profile of extraordinary transmission of two-dimensional nanohole arrays in a metal film.[13] Very recently, Fano resonances have been observed in plasmonic nanocavities[16−18,21−23] and nanoclusters[24−29] in which the discrete and continuum states in an atomic or molecular system are mimicked, respectively, by a "dark" quadruple mode or a subradiant mode with a very narrow linewidth and a "bright" or a superradiant one having a broad spectrum response. The sharp dispersion of Fano resonances in the aforementioned plasmonic nanostructures promises applications in lasing, switching, nonlinear and slowing-light devices, particularly in biosensing.[26,32] However, it lacks a general method to control flexibly the Fano profile featured by its linewidth and spectral

Received: January 28, 2012
Revised: March 20, 2012
Published: March 26, 2012

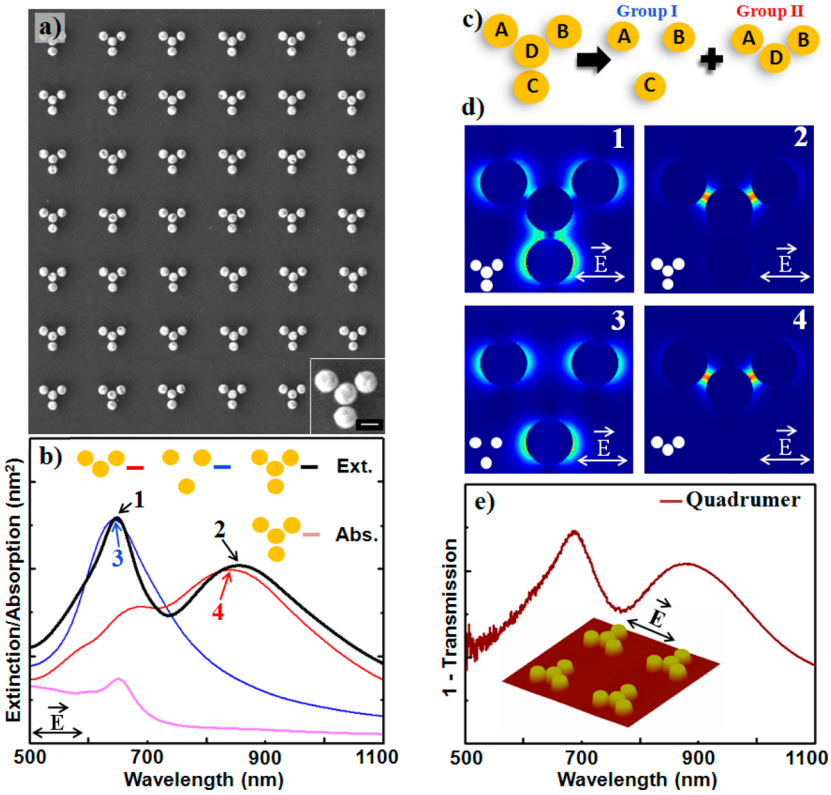

Figure 1. Subgroup decomposition of the spectral profile in plasmonic quadrumers. (a) SEM image of the fabricated periodic array of quadrumers consisting of Au disks. The scale bar is 100 nm. (b) Simulated extinction and absorption spectra of an individual quadrumer (black and pink curves) and the two subgroups (blue and red curves.) (c) Sketch of decomposing a quadrumer into Groups I and II. (d) Electric field intensity distribution in the quadrumer at peaks 1 and 2 and in the two subgroups at their respective extinction peaks 3 and 4. (e) Measured extinction spectrum of the quadrumer array at normal incidence. The inset shows the three-dimensional AFM image of the quadrumers and the incident polarization.

contrast, which in fact largely determine the overall performance of Fano-resonance-based devices, such as the detection limit of a biosensor employing this type of resonance. On the other hand, the strong hybridization feature at the Fano dip in nanoclusters prevents an intuitively understanding and designing of the overall profile because the individual components are usually shared by the sharp and broad resonances.[24−29] A significant step forward was recently done by Halas and coworkers[33] in order to explain the difference observed between the spectra obtained with electron-beam or with plane wave excitation. They discovered that a deconstruction of the nanocluster is possible; such a deconstruction was given by the superposition of a subradiant and a superradiant state of the system.

In this Letter, we describe a general recipe that allows one to tailor easily but significantly the overall spectral profile in plasmonic nanoclusters. We show that the spectral shape of resonances in plasmonic pentamers and quadrumers can be decoded into two individual contributions from their subgroups. Remarkably, in the particularly considered systems, such subgroups are not due to the superposition of a subradiant and a superradiant state as described in ref 32, but they are the real eigenstates of the subgroups whose interference gives rise to the resonance lineshape. More specifically, we observe that the spectrum arises from the efficient excitations of the two subgroups, which is confirmed by the near field distribution in the system at the relevant resonance positions and the calculation of the scattered field by each subgroup. This observation enables us to tune and design the overall resonance lineshape by selectively altering the particle shape of either subgroup without a need to change the particle size, interparticle distance or the number of elements of the oligomers. On the basis of this finding, we demonstrate large spectral shifts (either red or blue) and significant changes in spectral contrast and linewidth of hybridized plasmon resonances when varying the particle geometry of one subgroup in quadrumers and pentamers, which are particularly important for plasmonic nanosensors. This novel understanding of the optical response of plasmonic nanoclusters captures some physical aspects beyond the well-known interference mechanism, which could bring about the new scope of plasmonic-nanocluster-based applications.

We have fabricated arrays of Au quadrumers and pentamers consisting of differently shaped components on the same quartz substrate by electron beam lithography (Elonix 100KV EBL system). Each array has a dimension of 50 × 50 μm^2 and consists of 60 nm thick Au nanoparticles. Three nanometer thick Ti film was deposited on the substrate by e-beam evaporation (EB03 BOC Edwards) to increase the adhesion between Au and quartz, followed by an evaporation of 60 nm Au film and a spin-coating of 50 nm hydrogen silsesquioxane (HSQ) as a negative electro-resist. After baking the sample at 200 °C for 2 min, a combined process of e-beam exposure, chemical development, and ion-milling was performed to create well-defined Au oligomers on the substrate. The surface morphology of fabricated structures was characterized by high-resolution scanning electron microscopy (SEM) and atomic force microscopy (AFM). Figure 1a (2a) shows the SEM image of a quadrumer (pentamer) array consisting of circular nanodisks, exhibiting the repeatable high-quality of the

dx.doi.org/10.1021/nl3003683 | Nano Lett. 2012, 12, 2101−2106

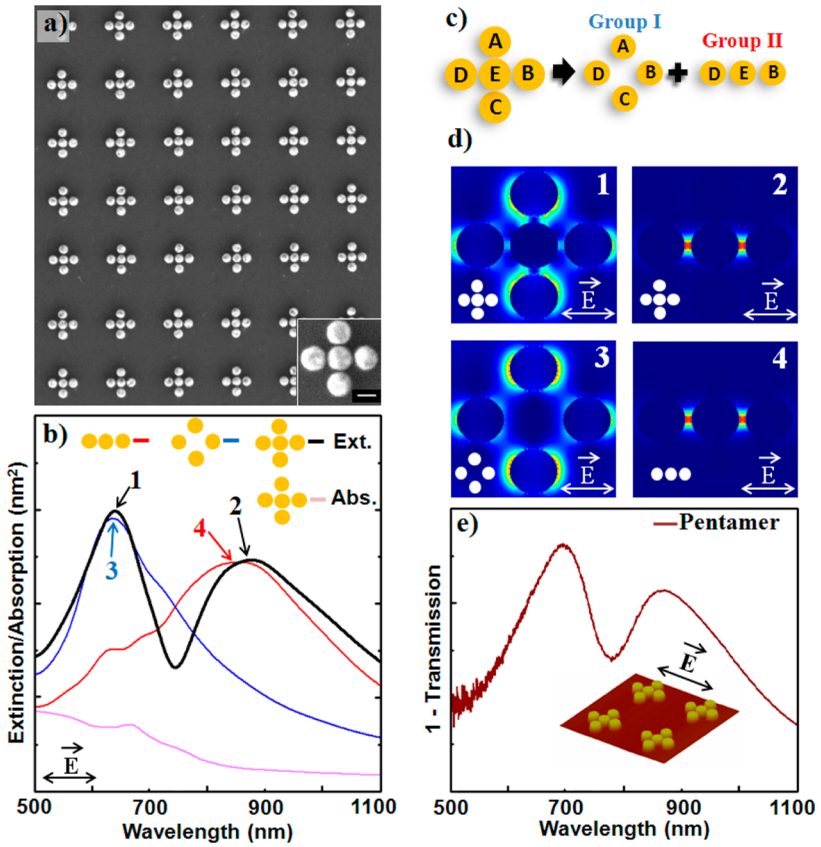

Figure 2. Subgroup decomposition concept applied to plasmonic pentamers. (a) SEM image of a periodic array of pentamers consisting of Au disks. The scale bar is 100 nm. (b) Simulated extinction and absorption spectra of an individual pentamer (black and pink curves) and the two subgroups (blue and red curves). (c) Sketch of decomposing a pentamer into Groups I and II. (d) Electric field intensity distribution in the pentamer at peaks 1 and 2 and in the two subgroups at their respective extinction peaks 3 and 4. (e) Measured extinction spectrum of the pentamer array at normal incidence. The inset shows a 3D AFM image of the pentamers and the incident polarization.

sample over a large area. In addition, AFM imaging as shown in the insets of Figures 1e and 2e reveals a good preservation of the particle shape from the top to bottom surface.

Three-dimensional (3D) simulations were performed to calculate the extinction cross sections of individual nanostructures by using a commercially available finite-difference-time-domain code (Lumerical FDTD). The dielectric functions of Au used in the simulations were extracted from Johnson and Christy data.[34] Different from many previous studies,[24−29] a full consideration of the substrate effect was made in our simulations, which resulted in a good agreement between simulation and experiment. Fourier transform infrared spectroscopy (FTIR, Bruker Hyperion 2000) was used to measure the extinction, defined as (1 - Transmission), through the arrays at normal incidence with a linear polarization. Figure 1a shows an array of quadrumers consisting of 140 nm diameter circular-shaped disks with 20 nm interparticle distance and Figure 1e the measured extinction spectrum. This agrees very well with the simulated spectrum as shown in Figure 1b (black line). Both spectra are dominated by a remarkable extinction dip, which on first glance could be classified as a Fano resonance, akin to previous investigations of nanocluster systems.[24−29] Such a Fano resonance occurs due to the destructive interference between a superradiant mode arising from the dipole moments of all the components oriented parallel to each other and a subradiant mode where the dipole orientations are antiparallel.

In this work, we take a different perspective to understand the overall spectral characteristics of our nanoclusters. Instead of exploring the formation mechanism of the extinction dip, we focus our attention on the origin of the two peaks. A useful clue is that the two dominant peaks in Figure 1b seem to be well described by two separate resonances given by two subgroups (see Figure 1c). This intuition is further confirmed by calculating the electric-field intensity distribution in the quadrumer at the two peak wavelengths. The top panel of Figure 1d clearly demonstrates that at the first peak position, the three outer disks are efficiently excited inducing strong field enhancements around each particle while the center disk is relatively dark. Such a selective excitation of different particles is even more pronounced at the second peak position where the upper three disks become dominant, leaving the bottom one completely dark. On the basis of these observations, we propose that the complex optical excitation in the whole quadrumer structure can be decomposed into two separate contributions from its subgroups, group I consisting of the outer three disks and group II of the upper three disks (see Figure 1c). Following this idea, we calculate the extinction of the two subgroups separately (blue and red lines in Figure 1b) and we compare them with the extinction of the full nanostructure (black line in Figure 1b). Note that the curves in Figure 1b are in the same units. Indeed, the extinction spectra from the two subgroups overlap well with the two peaks of the quadrumer extinction spectrum in terms of both the position and amplitude (see Figure 1b), demonstrating that the

dx.doi.org/10.1021/nl3003683 | *Nano Lett.* 2012, 12, 2101−2106

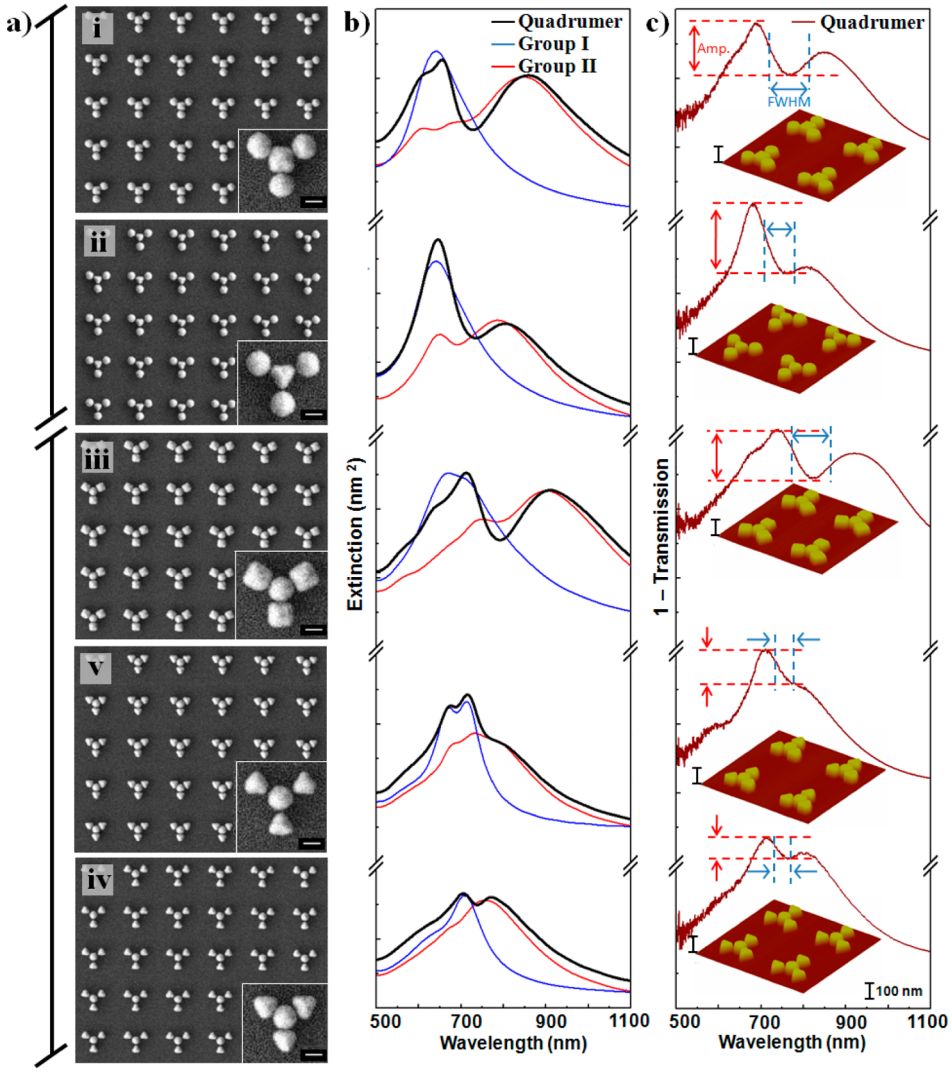

Figure 3. Systematic modification of plasmon resonance lineshape in various quadrumers. (a) SEM images of hybrid quadrumers consisting of differently shaped elements. The scale bar in each image is 100 nm. (b) Simulated extinction spectra for the quadrumers (black curve) and their two subgroups (blue and red curves). (c) Measured extinction spectra for the same quadrumers at normal incidence, along with 3D AFM images of the nanostructures.

overall spectral response of the quadrumer is due to the interaction of the separate excitations of the subgroups at different wavelength ranges. Curiously, results in Figure 1b suggest that the interaction of the two subgroups is such that each subgroup is not active at the same range of frequencies; instead the first part of the spectrum is dominated by the group I and the second part by the group II (see Figure 1b). In other words, the total spectrum of the quadrumer is the convolution of the two separate subspectra. Note also that at the peak frequencies the electric near-field distribution of each subgroup is very similar to that obtained for the complete nanocluster (see Figure 1d), confirming the decomposition assumption. Further calculation of the absorption spectrum for the quadrumer does not show an absorption peak at the corresponding extinction dip (see Figure 1b), which usually appears for a plasmonic Fano resonance in large nanoclusters, such as heptamers, due to the strong absorption of the subradiant mode that interferes with the superradiant one.[24−27] This observation confirms the very weak interaction between the two eigenstates of the two subgroups, and hence the observed extinction dip cannot be reasonably classified as a plasmonic Fano resonance.

The same idea can be applied to understand the optical properties of other plasmonic oligomers, such as pentamers, as shown in Figure 2. Similar to the quadrumer case, guided by the near-field distribution at the peak frequencies, a pentamer can be deconstructed into two individual subgroups, group I consisting of the outer four disks and group II of the three ones in the middle (see Figure 2c). Again, as depicted in Figure 2b, the extinction spectra of these two subgroups are in very good agreement with the overall spectral response of the pentamer, which indicates the selective excitation of either group at the respective resonance wavelength. Such a selective excitation is further confirmed by comparing the near-field distribution between the subgroups and the whole structure. As can be seen from Figure 2d, at the first peak position, the outer four disks in the pentamer are strongly excited while the center one is relatively inactive, which is equivalent to modal excitation of subgroup I. In contrast, at the second peak position, only the three disks in the middle of the pentamer are excited, exhibiting an electric-field distribution that resembles that of the second

dx.doi.org/10.1021/nl3003683 | *Nano Lett.* 2012, 12, 2101−2106

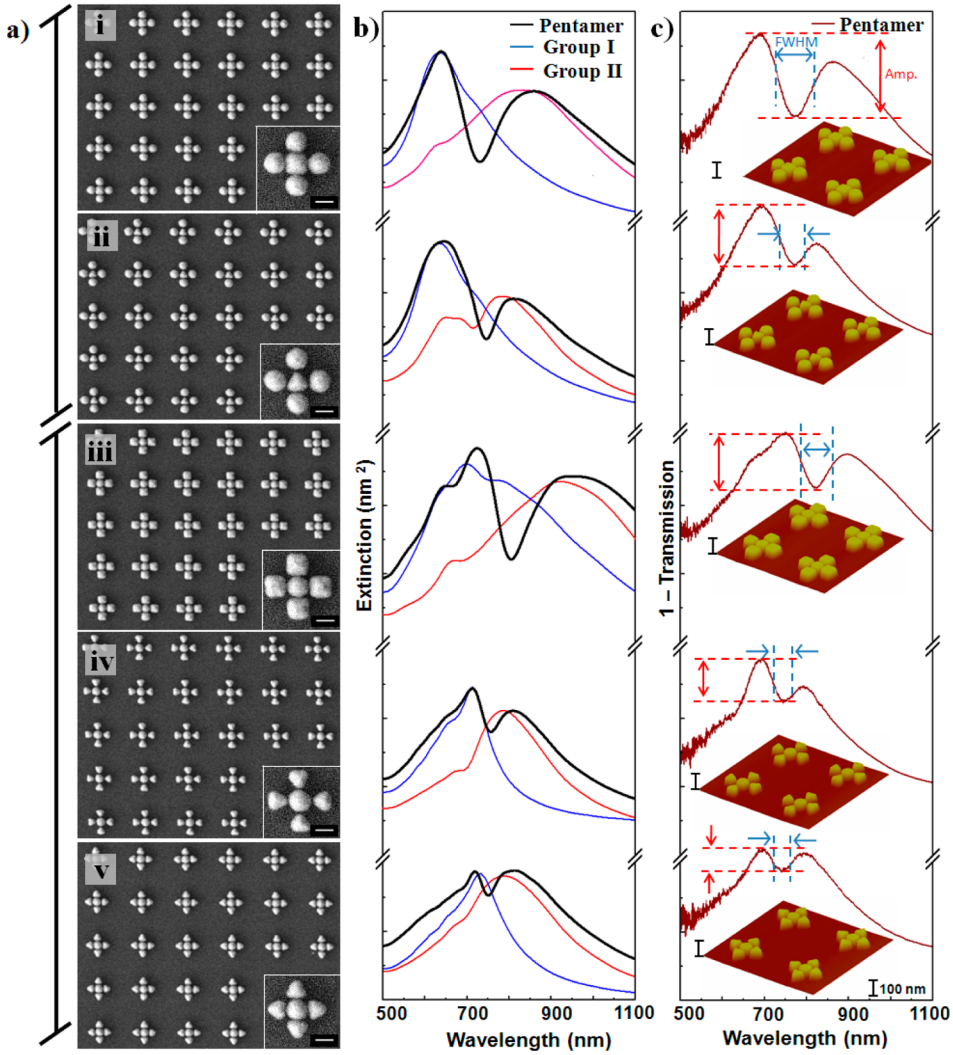

Figure 4. Tuning of resonance linewidth and spectral contrast of plasmon resonances in different pentamers. (a) SEM images of hybrid pentamers consisting of differently shaped elements. The scale bar in each image is 100 nm. (b) Simulated extinction spectra for the pentamers (black curve) and their two subgroups (blue and red curves). (c) Measured extinction spectra for the same pentamers at normal incidence, along with 3D AFM images of the nanostructures.

subgroup. Figure 2e shows the measured extinction spectrum of the pentamer array that is consistent with the simulated result in Figure 2b, characterized by a sharp extinction dip in both spectra. Actually, the main difference between the quadrumers (Figure 1) and pentamers (Figure 2) is the interference strength between the two subgroups. In fact, we can see that in the pentamer case destructive interference between the modes of two subgroups with different linewidths leads to a more pronounced extinction dip, as well as a small resonance shift and linewidth variation, while in the quadrumers the subgroup modes are almost unmodified. The pentamer case in some aspect is similar to the recent results reported by Halas and co-workers,[33] where the nanocluster decomposition is due to the superposition of superradiant and subradiant modes. In addition, our calculation shows that a weak absorption shoulder appears at the extinction dip position for pentamers (see Figure 2b), which evidences an appreciable destructive interference between the broad mode of subgroup 2 and the weak extinction shoulder of subgroup 1 occurring in the proximity of the extinction dip of pentamers.

Understanding the nature of the spectral response in nanoclusters is a key point for intuitive design of the resonance lineshape. For instance, we will see in the following some examples of how to use the oligomer decomposition idea for spectral modification. Having the quadrumer decomposition of Figure 1c as a starting point, we can for example change the central particle shape and in this way we modify only the optical property of group II, that is, only the second resonance (red curve Figure 1b) but leaving the first one unmodified (blue curve Figure 1b). Also we can change, for example, only the external nanoparticles, modifying in this way both groups. Those situations are shown in Figure 3. We can see that by changing the shape of the nanoparticle but leaving the particle size and interparticle distance constant a flexible remodeling of the overall spectral shape is obtained, manifested by a systematic variation in the relative height of the two peaks as well as the resonance linewidth of the spectral dip. More specifically, replacing the center circularly shaped disk of the quadrumer shown in Figure 1 by a square- or triangle-shape nanodisk allows for significant tuning of the peak-dip contrast and the resonance full-width-at-half-maximum (FWHM) (see the first two cases in Figure 3), which are two crucial parameters for realizing high-resolution plasmonic biosensors. More pronounced modification of the spectral profile can be

dx.doi.org/10.1021/nl3003683 | *Nano Lett.* 2012, 12, 2101–2106

obtained by changing the particle shape of the outer three disks in the quadrumer (see the last three cases in Figure 3) because the spectral response of both subgroups is altered in this way. In addition, it is also possible to modify the particle size and interparticle distance of the subgroups, and hence open two extra degrees of freedom in the spectral design, which are particularly important for shifting the peak or dip positions. The same design scheme can be applied to the case of pentamers (see Figure 4), and as already shown in this case the stronger destructive interference gives rise to a pronounced extinction dip. Note that for the pentamers the destructive interference is stronger when the first group (blue curves) presents a shoulder (first three cases of Figure 4). For example, we can design two subgroups with very different linewidths, stressing in such case the asymmetric lineshape of the total structure. It is worthwhile to note that the different degree of interference obtained for the quadrumers and pentamers seems linked to the different degree of the nanocluster symmetry. This can be an extra valuable parameter important for modeling the spectrum that deserves further studies.

In conclusion, we have shown that nanocluster extinction spectra of quadrumers and pentamers can be associated to different degrees of interference strength of eigenmodes of two nanoparticle subgroups. On the basis of that observation, the nanocluster spectral response can be analyzed and designed by changing the particle shape of either subgroup separately or simultaneously, thereby offering a powerful and flexible method to control the resonance lineshape systematically without invoking a change of particle size, interparticle distance, or the number of elements of the oligomers. It is also important to note that unlike systems with strong Fano interferences, for the quadrumer case the subgroup interference is so weak that each subgroup is active at a particular frequency range where the other is inactive, leading in this way a final spectrum that is the exact convolution of the two subspectra.

AUTHOR INFORMATION

Corresponding Author

*E-mail: (M.H.) elehmh@nus.edu.sg; (S.A.M.) s.maier@imperial.ac.uk.

Author Contributions

¶M.R. and D.Y.L. contributed equally to this work.

Notes

The authors declare no competing financial interest.

ACKNOWLEDGMENTS

The authors acknowledge funding provided by SERC Agency of Science, Technology and Research (A*STAR) Superlens Program (Project No. 092 154 0099) and the UK EPSRC. M.R. would like to express his gratitude for the support from the A*STAR − SINGA program. D.Y.L. acknowledges the funding from the Leverhulme Trust.

REFERENCES

(1) Fano, U. *Phys. Rev.* **1961**, *124*, 1866−1878.
(2) Fano, U. *Nuovo Cimento* **1935**, *12*, 154−161.
(3) Rousseau, D. L.; Porto, S. P. S *Phys. Rev. Lett.* **1968**, *20*, 1354−1357.
(4) Nitzan, A.; Jortner, J. *Mol. Phys.* **1972**, *24*, 109−131.
(5) Luo, H. G.; Xiang, T.; Wang, X. Q.; Su, Z. B.; Yu, L. *Phys. Rev. Lett.* **2004**, *92*, 256602.
(6) Johnson, A. C.; Marcus, C. M.; Hanson, M. P.; Gossard, A. C. *Phys. Rev. Lett.* **2004**, *93*, 106803.
(7) Kobayashi, K.; Aikawa, H.; Sano, A.; Katsumoto, S.; Iye, Y. *Phys. Rev. B* **2004**, *70*, 035319.
(8) Rybin, M. V.; Khanikaev, A. B.; Inoue, M.; Samusev, K. B.; Steel, M. J.; Yushin, G.; Limonov, M. F. *Phys. Rev. Lett.* **2009**, *103*, 023901.
(9) Miroshnichenko, A. E.; Flach, S.; Kivshar, Y. S. *Rev. Mod. Phys.* **2010**, *82*, 2257−2298.
(10) Luk'yanchuk, B.; Zheludev, N. I.; Maier, S. A.; Halas, N. J.; Nordlander, P.; Giessen, H.; Chong, C. T. *Nat. Mater.* **2010**, *9*, 707−715.
(11) Maier, S. A. *Plasmonics: Fundamentals and Applications*; Springer: Berlin, 2007.
(12) Christ, A.; Tikhodeev, S. G.; Gippius, N. A.; Kuhl, J.; Giessen, H. *Phys. Rev. Lett.* **2003**, *91*, 183901.
(13) Genet, C.; Van Exter, M. P.; Woerdman, J. P. *Opt. Commun.* **2003**, *225*, 331−336.
(14) Lee, H. T.; Poon, A. W. *Opt. Lett.* **2004**, *29*, 5−7.
(15) Luk'yanchuk, B. S.; Tribelsky, M. I.; Ternovsky, V.; Wang, Z. B.; Hong, M. H.; Shi, L. P.; Chong, T. C. *J. Opt. A: Pure Appl. Opt.* **2007**, *9*, S294−S300.
(16) Zhang, S.; Genov, D. A.; Wang, Y.; Liu, M.; Zhang, X. *Phys. Rev. Lett.* **2008**, *101*, 047401.
(17) Bachelier, G.; Russier-Antoine, I.; Benichou, E.; Jonin, C; Del Fatti, N.; Vallée, F.; Brevet, P.-F. *Phys. Rev. Lett.* **2008**, *101*, 197401.
(18) Hao, F.; Sonnefraud, Y.; Van Dorpe, P.; Maier, S. A.; Halas, N. J.; Nordlander, P. *Nano Lett.* **2008**, *8*, 3983−3988.
(19) Neubrech, F.; Pucci, A.; Cornelius, T. W.; Karim, García-Etxarri, A.; Aizpurua, J. *Phys. Rev. Lett.* **2008**, *101*, 157403.
(20) Parsons, J.; Hendry, E.; Sambles, J. R.; Barnes, W. L. *Phys. Rev. B* **2009**, *80*, 245117.
(21) Verellen, N.; Sonnefraud, Y.; Sobhani, H.; Hao, F.; Moshchalkov, V. V.; Van Dorpe, P.; Nordlander, P.; Maier, S. A. *Nano Lett.* **2009**, *9*, 1663−1667.
(22) Pryce, I. M.; Aydin, K.; Kelaita, Y. A.; Briggs, R. M.; Atwater, H. A. *Nano Lett.* **2010**, *10*, 4222−4227.
(23) Sonnefraud, Y.; Verellen, N.; Sobhani, H.; Vandenbosch, G.; Moshchalkov, V. V.; Van Dorpe, P.; Nordlander, P.; Maier, S. A. *ACS Nano* **2010**, *4*, 1664−1670.
(24) Fan, J. A.; Wu, C.; Bao, K.; Bao, J.; Bardhan, R.; Halas, N. J.; Manoharan, V N.; Nordlander, P.; Shvets, G.; Capasso, R. *Science* **2010**, *328*, 1135−1138.
(25) Hentschel, M.; Saliba, M.; Vogelgesang, R.; Giessen, H.; Alivisatos, A. P.; Liu, N. *Nano Lett.* **2010**, *10*, 2721−2726.
(26) Lassiter, J. B.; Sobhani, H.; Fan, J. A.; Kundu, J.; Capasso, F.; Nordlander, P.; Halas, N. J. *Nano Lett.* **2010**, *10*, 3184−3189.
(27) Fan, J. A.; Wu, C.; Bao, K.; Wu, C.; Bao, J.; Bardhan, R.; Halas, N. J.; Manoharan, V N.; Shvets, G.; Nordlander, P.; Capasso, R. *Nano Lett.* **2010**, *10*, 4680−4685.
(28) Rahmani, M.; Tahmasebi, T.; Lin, Y.; Luk'yanchuk, B.; Liew, T. Y. F.; Hong, M. H. *Nanotechnology* **2011**, *22*, 245204.
(29) Hentschel, M.; Dregely, D.; Vogelgesang, R.; Giessen, H.; Liu, N. *ACS Nano* **2011**, *5*, 2042.
(30) Lei, D. Y.; Li, J.; Fernandez-Dominguez, A. I.; Ong, H. C.; Maier, S. A. *ACS Nano* **2010**, *4*, 432−438.
(31) Giannini, V.; Francescato, Y.; Amrania, H.; Phillips, C. C.; Maier, S. A. *Nano Lett.* **2011**, *11*, 2835−2840.
(32) Yanik, A. A.; Cetin, A. E.; Huang, M.; Artar, A.; Hossein Mousavi, S.; Khanikaev, A.; Connor, J. H.; Shvets, G; Altug, H. *Proc Natl. Acad. Sci. U.S.A.* **2010**, *108*, 11784−11789.
(33) Lassiter, J. B.; Sobhani, H.; Knight, M. W.; Mielczarek, W. S.; Nordlander, P.; Halas, N. J. *Nano Lett.* **2012**, *12* (2), 1058−1062.
(34) Johnson, P. B.; Christy, R. *Phys. Rev. B* **1972**, *6*, 4370−4379.